ELSEVIER

Catalysis Today 78 (2003) 561–569

CATALYSIS TODAY

www.elsevier.com/locate/cattod

Photocatalytic water splitting into H_2 and O_2 over various tantalate photocatalysts

Hideki Kato, Akihiko Kudo*

Department of Applied Chemistry, Faculty of Science, Science University of Tokyo, 1-3 Kagurazaka, Shinjuku-ku, Tokyo 162-8601, Japan

Abstract

Photocatalytic water splitting into H_2 and O_2 over various tantalates was reviewed and factors affecting photocatalytic activities of tantalates were discussed from a viewpoint of the crystal structure and the energy structure. Many tantalates, $K_3Ta_3Si_2O_{13}$, alkali and alkaline earth tantalates, were highly active photocatalysts for water splitting. The high activities were mainly due to the high conduction band level consisting of Ta5d orbitals. NiO-loaded $NaTaO_3$ with the distorted perovskite structure showed the highest activity among tantalates. Moreover, the activity of the NiO/$NaTaO_3$ photocatalyst was remarkably improved by doping of lanthanoids. The apparent quantum yield of NiO/$NaTaO_3$ doped with lanthanum was ca. 50% at 270 nm.

Keywords: Photocatalytic water splitting; Tantalates; Lanthanum-doped $NaTaO_3$

1. Introduction

Photocatalytic water splitting has been extensively studied from a viewpoint of the photon energy conversion. It has been reported that some metal oxides show reasonable activities for water splitting into H_2 and O_2 in a stoichiometric ratio under UV light irradiation [1–9]. However, the number of photocatalyst materials found is still limited and active materials being employed are mainly titanates. Therefore, further investigation of the photocatalyst materials for water splitting is indispensable for revealing essential factors of active photocatalysts and getting a guiding principle of development of new photocatalyst materials.

Tantalates possess conduction bands consisting of Ta5d orbitals at more negative position than titanates (Ti3d) and niobates (Nb4d). Such a high potential of the conduction band should be advantageous to reduction of water to produce H_2. On the other hand, there are many reports for photoluminescence of tantalates [10–16]. It suggests that tantalates are photoactive materials with good photophysical properties. However, there are few reports for photocatalytic activities of tantalates [5]. These facts let the authors study systematically on photocatalytic water splitting over tantalates.

In the present paper, photocatalytic water splitting over various tantalates investigated by the authors is reviewed.

2. Experimental

Various tantalates were prepared by conventional solid state reactions and flux methods using a borate flux. The starting materials (carbonates and oxides) were mixed in a mortar and the mixtures were calcined in air. In the preparation of alkali tantalates, the excess amount of alkali was added to compensate the volatilization. The excess alkali was washed out

* Corresponding author. Fax: +81-3-3235-2214.
E-mail address: a-kudo@rs.kagu.tus.ac.jp (A. Kudo).

0920-5861/02/$ – see front matter
PII: S0920-5861(02)00355-3

with water after the preparation. The obtained powders were confirmed by X-ray diffraction using Cu Kα radiation (Rigaku; RINT-1400). NiO co-catalysts were loaded by an impregnation method from aqueous solutions of $Ni(NO_3)_2{\cdot}6H_2O$ (Wako Pure Chemical; 98.0%). The photocatalysts loaded with the NiO co-catalyst by an impregnation method were calcined at 540–720 K in air. The pretreatment, reduction with H_2 (200 Torr) at 520 or 770 K for 2 h followed by oxidation with O_2 (100 Torr) at 470 or 770 K for 1 h, was carried out for NiO-loaded photocatalysts, if necessary.

Photocatalytic reactions were carried out in a gas-closed circulation system. The photocatalyst powder was dispersed in pure water by a magnetic stirrer in an inner irradiation cell made of quartz. In some cases, NaOH was added into a reactant solution. The light source was a 400 W high-pressure mercury lamp (SEN; HL400EH-5). Apparent quantum yields were measured using a 300 W Xe illuminator (ILC Technology; CERMAX-LX300) attached with a band pass filter (Kenko; BPUV-270, WHM: 16 nm). The number of reacted electrons was determined from the amount of evolved H_2. The number of incident photons was measured by a chemical actinometry employing ammonium ferrioxalate. The amounts of H_2 and O_2 evolved were determined using gas chromatography (Shimadzu; GC-8A, MS-5A column, TCD, Ar carrier).

Diffuse reflection spectra were obtained using a UV-Vis-NIR spectrometer (Jasco; UbestV-570) and were converted from reflection to absorbance by the Kubelka–Munk method. Photoluminescence was measured in vacuo using a spectrofluorometer (Spex; FluoroMax). Surface areas were determined by BET measurement (Coulter; SA3100). Photocatalyst powders were observed by a scanning electron microscope (Hitachi; S-5000).

3. Results and discussion

3.1. Photocatalytic activities of $K_3Ta_3Si_2O_{13}$ with a pillared structure consisting of three TaO_6 chains [17]

$K_3M_3Si_2O_{13}$ (M: Nb and Ta) possesses a unique pillared structure as shown in Fig. 1 [18]. Three MO_6 chains sharing the corners are bridged by ditetrahedral Si_2O_7 units. Band gaps of $K_3Nb_3Si_2O_{13}$ and $K_3Ta_3Si_2O_{13}$ were estimated to be 3.9 and 4.1 eV from the onsets of absorption, respectively. Photoluminescence was observed for $K_3Ta_3Si_2O_{13}$ at 77 K as shown in Fig. 2, whereas it was not observed for $K_3Nb_3Si_2O_{13}$. The onset of the excitation spectrum was around 300 nm and corresponded with that of the diffuse reflection spectrum.

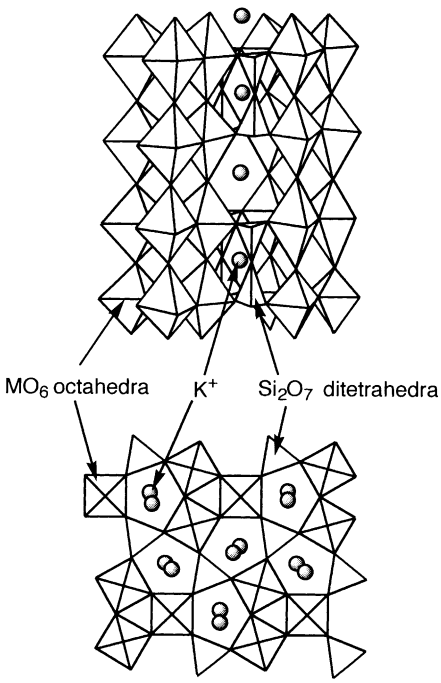

Fig. 1. Crystal structure of $K_3M_3Si_3O_{13}$ (M: Nb and Ta).

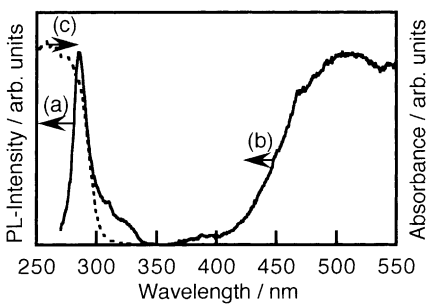

Fig. 2. Photoluminescence spectra of $K_3Ta_3Si_3O_{13}$ at 77 K: (a) an excitation spectrum monitored at 510 nm and (b) an emission spectrum excited at 285 nm, and (c) a diffuse reflection spectrum at 300 K.

Table 1
Photocatalytic activities of NiO(1.3 wt.%)-loaded $K_3Nb_3Si_2O_{13}$ and $K_3Ta_3Si_2O_{13}$ for water splitting[a]

Catalyst	NiO co-catalyst	Pretreatment[b]	Activity (μmol h^{-1})	
			H_2	O_2
$K_3Nb_3Si_2O_{13}$	No	No	0	0
$K_3Nb_3Si_2O_{13}$	Yes	R770-O470	1	0
$K_3Ta_3Si_2O_{13}$	No	No	43	19
$K_3Ta_3Si_2O_{13}$	Yes	No	368	188
$K_3Ta_3Si_2O_{13}$	Yes	R770	57	25
$K_3Ta_3Si_2O_{13}$	Yes	R770-O470	92	40
$K_3Ta_3Si_2O_{13}$	Yes	R770-O770	100	47

[a] Catalyst: 1 g, pure water: 350 ml, 400 W high-pressure mercury lamp, inner irradiation cell made of quartz.
[b] R770 represents the reduction with H_2 (200 Torr) at 770 K for 2 h, R770-O470 and R770-O770 represent reduction with H_2 (200 Torr) at 770 K for 2 h followed by oxidation with O_2 (100 Torr) at 470 and 770 K for 1 h, respectively.

Table 1 shows photocatalytic activities of $K_3Nb_3Si_2O_{13}$ and $K_3Ta_3Si_2O_{13}$ for water splitting. $K_3Nb_3Si_2O_{13}$ showed no activities for water splitting while $K_3Ta_3Si_2O_{13}$ showed activities even without any co-catalysts such as Pt and NiO. Thus, differences in photoluminescence and photocatalytic properties between $K_3Nb_3Si_2O_{13}$ and $K_3Ta_3Si_2O_{13}$ were observed. The crystal structures of $K_3Nb_3Si_2O_{13}$ is similar to that of $K_3Ta_3Si_2O_{13}$. However, the M–O–M bond angles (M: Ta or Nb) in MO_6 chains of $K_3Ta_3Si_2O_{13}$ are 178° and 168° while those of $K_3Nb_3Si_2O_{13}$ are 174° and 167°. The ideal bond angle is 180°. The structure of $K_3Nb_3Si_2O_{13}$ is distorted more than that of $K_3Ta_3Si_2O_{13}$. The distortion of the framework and MO_6 octahedra strongly affects the energy structure of photocatalysts as mentioned in the next section and results in the differences in photoluminescence and photocatalytic properties between $K_3Nb_3Si_2O_{13}$ and $K_3Ta_3Si_2O_{13}$. On the other hand, the difference in the band gap between $K_3Nb_3Si_2O_{13}$ and $K_3Ta_3Si_2O_{13}$ is 0.2 eV: that is due to the difference in the conduction band level. 0.2 eV of the difference in the conduction band level can be enough to lead the drastic difference in the photocatalytic activity for water splitting between $K_3Nb_3Si_2O_{13}$ and $K_3Ta_3Si_2O_{13}$. Although the relationship between photoluminescent properties and photocatalytic activities is not so simple, many active photocatalysts, for example ZnO and CdS, show photoluminescence in the absence of reactants. The photoluminescence of $K_3Ta_3Si_2O_{13}$ would be ascribed to the recombination between photogenerated electrons and holes at some luminescent centers. In contrast, $K_3Nb_3Si_2O_{13}$ showed no photoluminescence even at 77 K. This indicates that the non-radiative transition readily occur in $K_3Nb_3Si_2O_{13}$ compared with $K_3Ta_3Si_2O_{13}$. The non-radiative transition is disadvantageous to the photocatalytic properties. Therefore, the photocatalytic activity of $K_3Nb_3Si_2O_{13}$ was negligible as shown in Table 1. It was noteworthy that the naked $K_3Ta_3Si_2O_{13}$ photocatalyst produced both H_2 (43 μmol h^{-1}) and O_2 (19 μmol h^{-1}) in a stoichiometric amount. When a NiO co-catalyst was loaded the activity was increased. However, any pretreatment resulted in the decrease in the activity. It has been reported that NiO was an efficient co-catalyst for photocatalytic water splitting [3,6–9,19]. Some NiO-loaded photocatalysts, such as TiO_2 [19], $SrTiO_3$ [8], and $K_2La_2Ti_3O_{10}$ [6], have been reported to be active for the water splitting. For all cases, the pretreatment of H_2 reduction followed by O_2 oxidation was indispensable for activation of the catalysts. The pretreatment makes the double layered structure of nickel in which metallic Ni and Ni oxide exist inside and on the external surface, respectively. The metallic Ni layer in the double layered structure assists the transfer of photogenerated electrons in the conduction bands of photocatalysts to NiO surface of a H_2 evolution site as shown in Fig. 3(b) [8]. In contrast to the NiO-loaded titanate photocatalysts, NiO/$K_3Ta_3Si_2O_{13}$ showed the high activity when such pretreatment was not performed. It was due to that the potential of the conduction band consisting of Ta5d orbitals was higher than those of titanates (Ti3d orbitals), resulting in that photogenerated electrons in the conduction band of $K_3Ta_3Si_2O_{13}$ were able to transfer NiO co-catalysts without the metallic Ni layer as shown in Fig. 3(c). Thus, the characteristics of $K_3Ta_3Si_2O_{13}$ were different from those of other reported photocatalysts and has arisen as a new type of the photocatalyst material for highly efficient water splitting into H_2 and O_2. The total amounts of electrons and holes reacted were more than the amount of the catalyst. These results clearly indicated that the reaction proceeded photocatalytically.

These results suggest that other tantalates of which conduction bands consist of Ta5d orbitals with high potentials be active for photocatalytic water splitting.

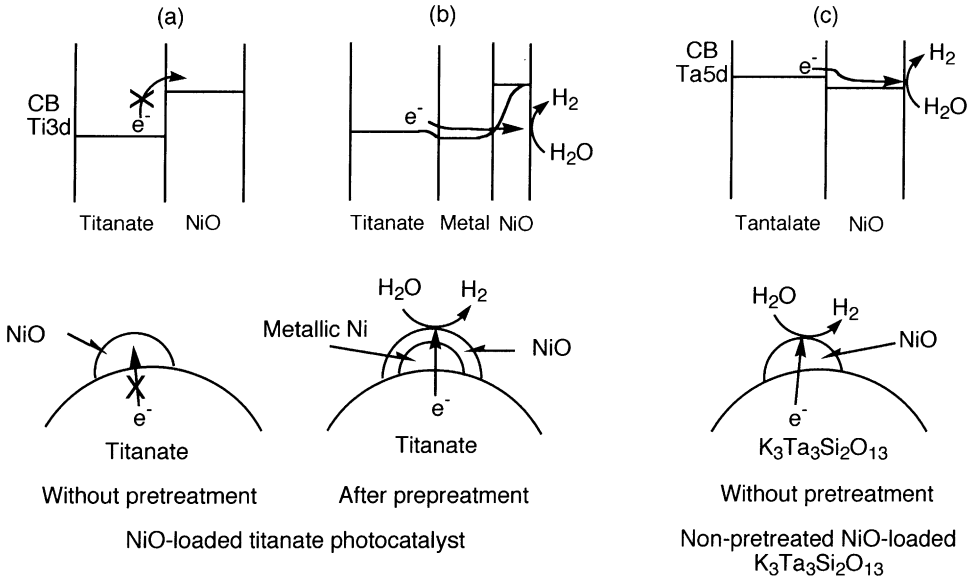

Fig. 3. Schemes of photogenerated electron transfer to the surface of NiO co-catalysts of NiO-loaded titanate and $K_3Ta_3Si_3O_{13}$ photocatalysts.

Therefore, further investigation was conducted using various tantalate materials.

3.2. *Photocatalytic activities of alkali tantalates $ATaO_3$ (A: Li, Na, and K) with perovskite-type structures [20,21]*

All of $ATaO_3$ (A: Li, Na, and K) consist of corner-sharing TaO_6 octahedra with perovskite-like structures as shown in Fig. 4. The bond angles of Ta–O–Ta are 143° ($LiTaO_3$) [22], 163° ($NaTaO_3$) [23], and 180° ($KTaO_3$) [24]. Wiegel et al. [14] have reported the relationship between crystal structures and energy delocalization for alkali tantalates $ATaO_3$ (A: Li, Na, and K). As the bond angle is close to 180°, migration of excited energy in the crystal occurs more easily and band gap becomes smaller. Therefore, the order of the delocalization of excited energy was

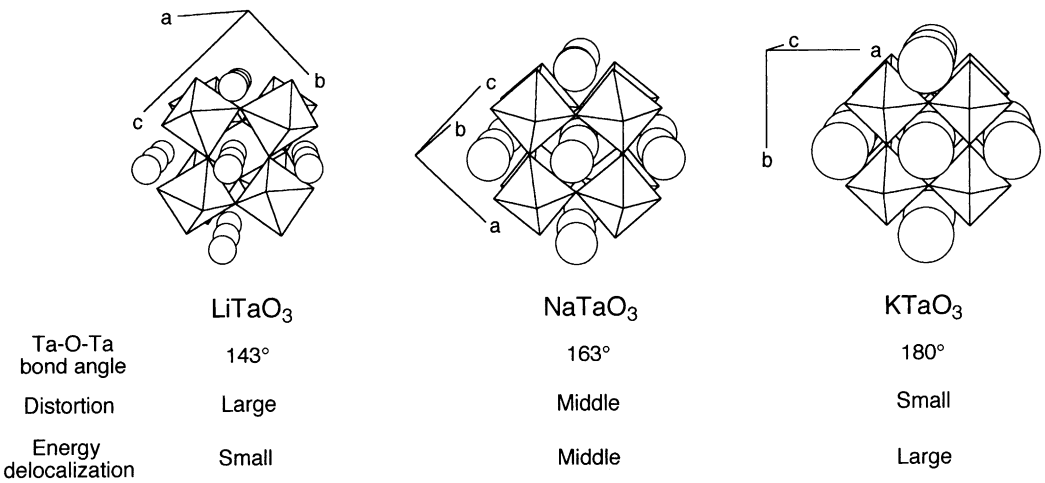

Fig. 4. Crystal structures of alkali tantalates $ATaO_3$ (A: Li, Na, and K) with perovskite-type structures.

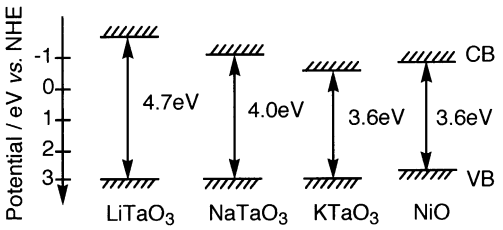

Fig. 5. Band structures of alkali tantalates $ATaO_3$ (A: Li, Na, and K) with perovskite-type structures.

$LiTaO_3 < NaTaO_3 < KTaO_3$, while that of band gap was reversed in the order as shown in Fig. 5. Here, the potentials of conduction bands were estimated by Eq. (1) reported by Scaife [25].

$$V_{fb} = 2.94 - E_g \quad (1)$$

Table 2 shows photocatalytic activities for water splitting into H_2 and O_2 in pure water on alkali tantalate photocatalysts with and without NiO co-catalysts. $NaTaO_3$ photocatalysts showed the highest photocatalytic activity when NiO co-catalysts were loaded. In this case, excess sodium in the starting material was indispensable for showing the high activity [20]. The conduction band level of the $NaTaO_3$ photocatalyst was higher than that of NiO (−0.96 eV) [26] as shown in Fig. 5. Moreover, the excited energy was delocalized in the $NaTaO_3$ crystal. Therefore, the photogenerated electrons in the conduction band of the $NaTaO_3$ photocatalyst were able to transfer to the conduction band of the NiO co-catalyst of an active site for H_2 evolution, resulting in the enhancement of the charge separation. Therefore, NiO-loading was effective for the $NaTaO_3$ photocatalyst even without special pretreatment. In contrast, the activity of $LiTaO_3$ was decreased by NiO-loading compared with that of naked $LiTaO_3$. It indicated that the low activity of $NiO/LiTaO_3$ was not due to the less number of absorbed photons but the inactivity of the NiO co-catalyst. The ability of the NiO co-catalyst was probably decreased by partly doping of Li^+ ions. The activity of the $KTaO_3$ photocatalyst was hardly enhanced by NiO-loading. It is due to the inability for the transfer of electrons photogenerated in $KTaO_3$ to NiO because of the low conduction band level. Thus, the high activity of $NiO/NaTaO_3$ is due to the suitable conduction band level consisting of Ta5d and energy delocalization caused by the proper distortion of TaO_6 connections. Fig. 6 shows photocatalytic water splitting over the NiO(0.05 wt.%)/$NaTaO_3$ photocatalysts in pure water and an aqueous NaOH solution (1 mmol l^{-1}). In the first run, the activity in pure water was higher than that in an aqueous NaOH solution. However, the activity in pure water was gradually decreased while that in an aqueous NaOH solution was stable. In the third and fourth runs, the activities in an aqueous NaOH solution were higher than those in pure water. It was found from the XRF and XPS measurement that the deactivation of NiO(0.05 wt.%)/$NaTaO_3$ was due to the elution and redeposition of nickel. The redeposited nickel widely covered the $NaTaO_3$ surface and it caused collapse of reaction sites and shielding of incident light. The

Table 2
Photocatalytic activities for water splitting on alkali tantalate photocatalysts[a]

Catalyst	Ratio of alkali to Ta[b]	Band gap[c] (eV)	Surface area ($m^2\,g^{-1}$)	Activity ($\mu mol\,h^{-1}$)	
				H_2	O_2
$LiTaO_3$	1.05	4.7	0.3	430	220
NiO(0.10 wt.%)/$LiTaO_3$	1.05	4.7	–	98	52
$NaTaO_3$	1.00	4.0	0.5	11	4.4
NiO(0.05 wt.%)/$NaTaO_3$	1.00	4.0	–	480	240
$NaTaO_3$	1.05	4.0	0.4	160	86
NiO(0.05 wt.%)/$NaTaO_3$	1.05	4.0	–	2180	1100
$KTaO_3$	1.10	3.6	1.6	29	13
NiO(0.10 wt.%)/$KTaO_3$	1.10	3.6	–	7.4	2.9

[a] Catalyst: 1 g, pure water: 350 ml, 400 W high-pressure mercury lamp, inner irradiation cell made of quartz.
[b] In starting materials.
[c] Estimated from the onset of absorption.

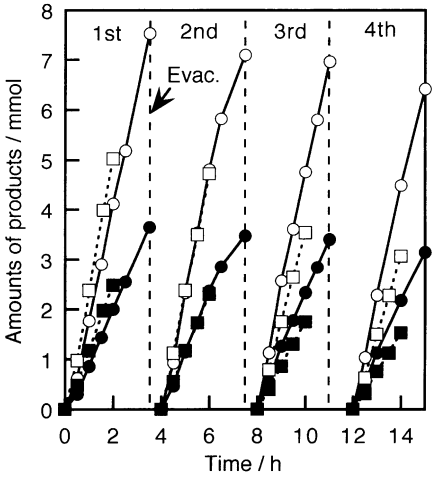

Fig. 6. Photocatalytic water splitting over NiO(0.05 wt.%)/$NaTaO_3$ photocatalysts in pure water (square) and in 1 mmol l^{-1} of an aqueous NaOH solution (circle). Catalyst: 1 g, reactant solution: 350 ml, 400 W high-pressure mercury lamp, inner irradiation cell made of quartz. Open marks: H_2, closed marks: O_2.

addition of the small amount of NaOH suppressed the elution of nickel, resulting in the steady reaction. Total amounts of H_2 and O_2 evolved from an aqueous NaOH solution were 28 and 14 mmol after 13 h of irradiation, respectively. The amounts of $NaTaO_3$ and NiO in 1 g of the NiO(0.05 wt.%)/$NaTaO_3$ photocatalyst were 4 mmol and 6.7 μmol, respectively. This strongly indicates that the water splitting proceeded photocatalytically on the NiO(0.05 wt.%)/$NaTaO_3$ photocatalyst. The apparent quantum yield of the NiO(0.05 wt.%)/$NaTaO_3$ photocatalyst was 20% at 270 nm.

3.3. *Photocatalytic activities of alkaline earth tantalates [27–30]*

Photophysical properties and photocatalytic activities of alkaline earth tantalates are summarized in Table 3. Orthorhombic alkaline earth tantalates $A'Ta_2O_6$ (A′: Ca, Sr, and Ba) consist of $CaTa_2O_6$-type structures as shown in Fig. 7(a). The order of photocatalytic activities of orthorhombic $A'Ta_2O_6$ without a NiO co-catalyst was $SrTa_2O_6$ > $BaTa_2O_6$ > $CaTa_2O_6$, and it corresponded to those of band gaps and the energy of photogenerated-electron/hole pairs transferring in the crystal (emission energy). The order of the band gaps of alkaline earth tantalates was

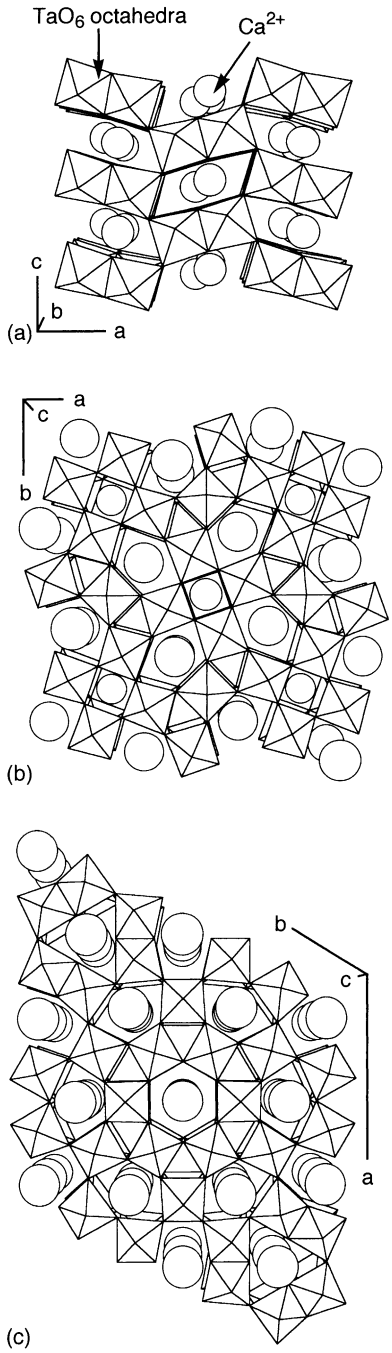

Fig. 7. Crystal structures of (a) orthorhombic $CaTa_2O_6$, (b) tetragonal $BaTa_2O_6$ and (c) hexagonal $BaTa_2O_6$.

Table 3
Photoluminescence properties and photocatalytic activities of alkaline earth tantalates[a]

Catalyst	Crystal structure	Band gap (eV)	Emission maximum[b] (nm)	Activity (μmol h^{-1})	
				H_2	O_2
$CaTa_2O_6$ (orthorhombic)	$CaTa_2O_6$	4.0	473	21	8.3
NiO(0.1 wt.%)/$CaTa_2O_6$ (orthorhombic)	–	–	–	72	32
$SrTa_2O_6$ (orthorhombic)	$CaTa_2O_6$	4.4	405	140	66
NiO(0.1 wt.%)/$SrTa_2O_6$ (orthorhombic)	–	–	–	960	490
$BaTa_2O_6$ (orthorhombic)	$CaTa_2O_6$	4.1	460	33	15
NiO(0.3 wt.%)/$BaTa_2O_6$ (orthorhombic)	–	–	–	629	303
$BaTa_2O_6$ (tetragonal)	Tetragonal tungsten bronze	3.8	505	14	6
NiO(0.4 wt.%)/$BaTa_2O_6$ (tetragonal)				53	28
$BaTa_2O_6$ (hexagonal)	Hexagonal tungsten bronze-related	4.0	515	7	2
NiO(0.4 wt.%)/$BaTa_2O_6$ (hexagonal)	–	–	–	21	10
$Sr_2Ta_2O_7$	Layered perovskite	4.6	450	53	18
NiO(0.15 wt.%)/$Sr_2Ta_2O_7$	–	–		1000	480

[a] Catalyst: 1 g, pure water: 350–390 ml, inner irradiation cell made of quartz, 400 W high-pressure mercury lamp.
[b] Observed at 77 K.

also $SrTa_2O_6$ > $BaTa_2O_6$ > $CaTa_2O_6$. Their valence bands are formed by O2p orbitals. These facts indicate that the conduction band level of $SrTa_2O_6$ is more negative than those of $BaTa_2O_6$ and $CaTa_2O_6$, suggesting that the potential of electrons photoexcited in $SrTa_2O_6$ is higher than those of $BaTa_2O_6$ and $CaTa_2O_6$. Therefore, the water splitting proceeded more easily over $SrTa_2O_6$ than $BaTa_2O_6$ and $CaTa_2O_6$. When the NiO co-catalysts were loaded, photocatalytic activities of all alkaline earth tantalates were increased. NiO/$SrTa_2O_6$ also showed a high activity among $A'Ta_2O_6$.

There are three crystal forms in $BaTa_2O_6$; orthorhombic of a low temperature form with a $CaTa_2O_6$-type structure, tetragonal of a medium temperature form with a tetragonal tungsten bronze structure [31], and hexagonal of a high temperature form with a hexagonal tungsten bronze-related structure [32] as shown in Fig. 7. The order of photocatalytic activities of three crystal phases of $BaTa_2O_6$ was an orthorhombic phase ≫ a tetragonal phase > a hexagonal phase as shown in Table 3. The order was different from that of band gaps. It was judged from the band gaps that the conduction band level of the hexagonal phase was more negative than that of the tetragonal phase. However, the order of the energy of photogenerated-electron/hole pairs transferring in the crystal (emission energy) of the $BaTa_2O_6$ was an orthorhombic phase ≫ a tetragonal phase > a hexagonal phase. The transferring excited energy of the hexagonal phase was slightly lower than that of the tetragonal phase. In addition, the transferring excited energy of the orthorhombic phase was remarkably larger than those of tetragonal and hexagonal phases. Therefore, it was considered that the transferring excited energy would mainly affect the photocatalytic activities of $BaTa_2O_6$ with three crystal phases.

NiO/$SrTa_2O_6$ was the most active photocatalyst among $A'Ta_2O_6$. An other strontium tantalate $Sr_2Ta_2O_7$ with a layered perovskite structure also showed the high activity (H_2: 1000 μmol h^{-1} and O_2: 480 μmol h^{-1}). $Sr_2Ta_2O_7$ showed the highest activity among alkaline earth tantalates. The quantum yield of the NiO(0.15 wt.%)/$Sr_2Ta_2O_7$ was 12% at 270 nm. $Sr_2Ta_2O_7$ did not possess an ion-exchange ability and the interlayer was not hydrated, indicating that both H_2 and O_2 evolution has to proceed at only the surface. Thus, the reaction mechanism on $Sr_2Ta_2O_7$ is different from that on $K_2La_2Ti_3O_{10}$ [6,8].

$Sr_2Ta_2O_7$ did not need any co-catalysts. Pretreatment was not necessary for NiO/$Sr_2Ta_2O_7$ to show the activity because of its high conduction band level. In contrast, NiO-loading and pretreatment were indispensable for obtaining the high activity of $Sr_2Nb_2O_7$ because the conduction band level of the oxide photocatalyst consisting of niobium was not so high generally [29]. Thus, the significant difference in photocatalytic properties between tantalates and

Table 4
Photocatalytic water splitting on NiO(0.05 wt.%)-loaded $NaTaO_3$:Ln(1 mol%) photocatalysts[a]

Ln-doped	Band gap (eV)	Surface area ($m^2\ g^{-1}$)	Activity (mmol h^{-1})	
			H_2	O_2
None	4.01	0.44	2.18[b]	1.10[b]
La	4.07	2.5	5.90	2.90
Pr	4.09	3.1	5.29	2.58
Nd	4.07	3.0	5.19	2.51
Sm	4.08	2.6	5.29	2.63
Eu	4.08	2.5	0.254	0.122
Gd	4.08	1.9	4.29	2.11
Tb	4.07	1.4	4.30	2.19
Dy	4.07	1.7	4.46	2.23
Yb	4.05	1.3	1.72	0.820

[a] Catalyst: 1 g, pure water: 390 ml, inner irradiation cell made of quartz, 400 W high-pressure mercury lamp.
[b] Initial activity.

niobates in the same family was observed as well as $K_3M_3Si_2O_{13}$ (M: Nb and Ta). Moreover, when a part of Ta in $Sr_2Ta_2O_7$ was replaced with Nb, the photocatalytic activity was drastically decreased [30].

3.4. Highly efficient photocatalytic water splitting into H_2 and O_2 over lanthanoids-doped $NaTaO_3$ [33]

$NiO/NaTaO_3$ showed the highest activity among alkali and alkaline earth tantalates. Table 4 shows band gaps, surface areas, and photocatalytic activities for water splitting into H_2 and O_2 in pure water on various lanthanide-doped $NaTaO_3$ (denoted as $NaTaO_3$:Ln hereafter) with NiO co-catalysts. $NaTaO_3$:Ln powders had larger surface areas than non-doped $NaTaO_3$. Band gaps of $NaTaO_3$:Ln were slightly higher than that of non-doped $NaTaO_3$. The activity of the $NiO/NaTaO_3$ photocatalyst was remarkably improved by doping of Ln, except for Eu and Yb. In the cases of $NaTaO_3$:Eu and Yb, doped Eu^{3+} and Yb^{3+} ions can trap the photogenerated electrons in the conduction band because Eu and Yb can take the divalent oxidation number. The electron trapping resulted in the decrease in photocatalytic activities. Moreover, the deactivation of the non-doped $NiO/NaTaO_3$ photocatalyst as shown in Fig. 6 was suppressed for the $NiO/NaTaO_3$:Ln photocatalysts even in pure water. $NiO/NaTaO_3$:La was the most active: H_2 and O_2 evolved steadily and efficiently as shown in Fig. 8. The optimized $NiO(0.2\ wt.\%)/NaTaO_3$:La(1.5%) photocatalyst evolved H_2 and O_2 with the rates of 14.6 and 7.2 mmol h^{-1}, respectively. The apparent quantum yield was ca. 50% at 270 nm. Thus, it was demonstrated that the photocatalytic water splitting was able to proceed efficiently using a photocatalyst powder system.

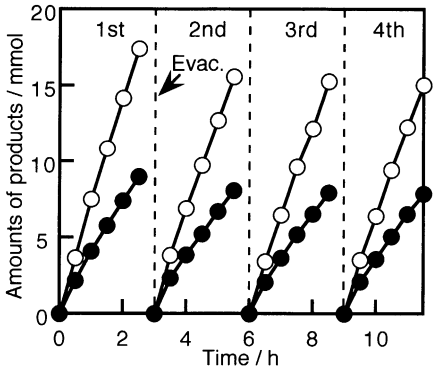

Fig. 8. Photocatalytic water splitting over NiO(0.05 wt.%)/$NaTaO_3$:La(1 mol%). Catalyst: 1 g, pure water: 390 ml, 400 W high-pressure mercury lamp, inner irradiation cell made of quartz. Open marks: H_2, closed marks: O_2.

It was found by SEM observation that the particle size of $NaTaO_3$:Ln powder, 0.1–0.7 μm, was remarkably smaller than that of non-doped $NaTaO_3$ powder, 2–3 μm. As the particle size is decreased, the probability of the surface reaction of electrons and holes with water molecules is increased in comparison with recombination in the bulk. On the other hand, a step structure was formed on the Ln-doped $NaTaO_3$ surface whereas the surface of non-doped $NaTaO_3$ was flat. The characteristic step structure might cause the separation of reaction sites. It was considered that these factors resulted in highly efficient photocatalytic water splitting over $NiO/NaTaO_3$:Ln.

4. Conclusions

(1) The photocatalytic activities of various tantalates for water splitting into H_2 and O_2 were investigated. It was found that many tantalates, $K_3Ta_3Si_2O_{13}$, alkali tantalates $ATaO_3$ (A: Li,

Na, and K), alkaline earth tantalates $A'Ta_2O_6$ (A′: Ca, Sr, and Ba) and $Sr_2Ta_2O_7$ evolved H_2 and O_2 from pure water under UV irradiation. Many of them showed activities even without any co-catalysts. Moreover, activities were drastically increased by loading of NiO co-catalysts even without pretreatment. They are characteristics of tantalate photocatalysts due to the high levels of conduction bands which consist of Ta5d orbitals. Among tantalate photocatalysts, $NiO/NaTaO_3$ showed the highest activity. The apparent quantum yield of $NiO/NaTaO_3$ photocatalyst was 20% at 270 nm. It was due to the suitable potential of the conduction band and delocalization of the excited energy caused by proper distortion of the TaO_6 connection.

(2) The relationship between photocatalytic activities and conduction band levels and/or transferring excited energy was observed for alkaline earth tantalates $A'Ta_2O_6$ (A′: Ca, Sr, and Ba) with $CaTa_2O_6$-type structures and the $BaTa_2O_6$ with three different crystal systems.

(3) The photocatalytic activity of $NiO/NaTaO_3$ were remarkably increased by doping of various lanthanoids except for Eu and Yb. Lanthanum was the most effective dopant among them. The optimized NiO(0.2 wt.%)/$NaTaO_3$:La(1.5%) photocatalyst showed the highest activity for water splitting into H_2 and O_2, H_2: 14.6 and O_2: 7.2 mmol h^{-1}, respectively. The apparent quantum yield of the $NiO/NaTaO_3$:La photocatalyst was 50% at 270 nm.

Acknowledgements

This work was supported by New Energy and Industrial Technology Development Organization (NEDO)/Research Institute of Innovate Technology for the Earth (RITE), Core Research for Evolutional Science and Technology (CREST), and a Grant-in-Aid (no. 11640601) from the Ministry of Education, Science, Sports, and Culture, Japan. One of us (H.K.) has been awarded a Research Fellowship of the Japan Society for the Promotion of Science for Young Scientists.

References

[1] K. Yamaguchi, S. Sato, J. Chem. Soc., Faraday Trans. I 81 (1985) 1237.
[2] J.-M. Lehn, J.-P. Sauvage, R. Ziessel, Nouv. J. Chim. 4 (1980) 623.
[3] A. Kudo, K. Sayama, A. Tanaka, K. Asakura, K. Domen, K. Maruya, T. Onishi, J. Catal. 120 (1989) 337.
[4] K. Sayama, H. Arakawa, J. Photochem. Photobiol. A 77 (1994) 243.
[5] K. Sayama, H. Arakawa, K. Domen, Catal. Today 28 (1996) 175.
[6] T. Takata, K. Shinohara, A. Tanaka, M. Hara, J.N. Kondo, K. Domen, J. Photochem. Photobiol. A 106 (1997) 45.
[7] H.G. Kim, D.W. Hwang, J. Kim, Y.G. Kim, J.S. Lee, Chem. Commun. (1999) 1077.
[8] K. Domen, J.N. Kondo, M. Hara, T. Takata, Bull. Chem. Soc. Jpn. 73 (2000) 1307.
[9] A. Kudo, J. Ceram. Soc. Jpn. 109 (2001) S81.
[10] A. Wachtel, J. Electrochem. Soc. 111 (1964) 534.
[11] G. Blasse, J. Solid State Chem. 72 (1988) 72.
[12] G. Blasse, L.H. Brixner, Mater. Res. Bull. 24 (1989) 363.
[13] G. Blasse, G.J. Dirksen, P. Zhiwu, G. Wehrum, R. Hoppe, Chem. Phys. Lett. 215 (1993) 363.
[14] M. Wiegel, M.H.J. Emond, E.R. Stobbe, G. Blasse, J. Phys. Chem. Solids 55 (1994) 773.
[15] M. Wiegel, W. Middel, G. Blasse, J. Mater. Chem. 5 (1995) 981.
[16] A.M. Srivastava, J.F. Ackerman, W.W. Beers, J. Solid State Chem. 134 (1997) 187.
[17] A. Kudo, H. Kato, Chem. Lett. (1997) 867.
[18] J. Choisnet, N. Nguyen, D. Groult, B. Raveau, Mater. Res. Bull. 11 (1976) 887.
[19] A. Kudo, K. Domen, K. Maruya, T. Onishi, Chem. Phys. Lett. 133 (1987) 517.
[20] H. Kato, A. Kudo, Catal. Lett. 58 (1999) 153.
[21] H. Kato, A. Kudo, J. Phys. Chem. B 105 (2001) 4285.
[22] S.C. Abrahams, J.L. Bernstein, J. Phys. Chem. Solids 28 (1967) 1865.
[23] M. Ahtee, L. Unonius, Acta Crystallogr. A 33 (1977) 150.
[24] E.A. Zhurova, V.E. Zavodnik, V.G. Trirel'son, Kristakkografiya 40 (1995) 816.
[25] D.E. Scaife, Solar Energy 25 (1980) 41.
[26] M.P. Dare-Edwards, J.B. Goodenough, A. Hamnett, N.D. Nicholson, J. Chem. Soc., Faraday Trans. II 77 (1981) 643.
[27] H. Kato, A. Kudo, Chem. Phys. Lett. 295 (1998) 487.
[28] H. Kato, A. Kudo, Chem. Lett. (1999) 1207.
[29] A. Kudo, H. Kato, S. Nakagawa, J. Phys. Chem. B 104 (2000) 571.
[30] H. Kato, A. Kudo, J. Photochem. Photobiol. A 145 (2001) 129.
[31] G.K. Layden, Mater. Res. Bull. 2 (1967) 533.
[32] G.K. Layden, Mater. Res. Bull. 3 (1968) 349.
[33] A. Kudo, H. Kato, Chem. Phys. Lett. 331 (2000) 373.